JOURNAL OF SOLID STATE CHEMISTRY 105, 223–233 (1993)

The Conditions for Detecting Confined Material in the Channels/Cavities of Zeolites by Using HREM

V. ALFREDSSON,* O. TERASAKI,† AND J.-O. BOVIN

National Center for HREM, Inorganic Chemistry 2, University of Lund, P.O. Box 124, S-221 00 Lund, Sweden; and †Department of Physics, Tohoku University, Sendai 980, Japan

Received April 6, 1992; in revised form November 16, 1992; accepted November 18, 1992

High resolution electron microscope images of zeolites recorded with the incident electron beam parallel to the main channels show an optical artifact. The contrast in the center of the channels is severely disturbed by dark spots caused by some Bragg reflections being insufficiently transferred by the objective lens. Since zeolites are being used as containers for other materials, the spots in electron micrographs will screen any materials located in the large zeolite channels. With experimental micrographs and image simulations it is shown that by changing the focus conditions the spot can be eliminated and hence, confined material can be imaged. Two representatives, mordenite and zeolite *Y*, are described in detail for the cases of one-dimensional and three-dimensional channel systems, respectively.

Introduction

Zeolites are used in a wide variety of applications such as selective catalysis, water adsorption, and ion-exchange. They can be represented by the general formula $M_{x/m}Si_{1-x}Al_xO_2 \cdot nH_2O$, where M is an exchangeable cation of valence m, and n is the number of water molecules. The zeolites investigated in this work were mordenite (MOR) and the ultrastable form of zeolite *Y* (FAU). The three capital letter notations follow the rules set up by a IUPAC Commission on Zeolite Nomenclature (*1*). Many of the important properties of zeolites are directly related to the framework structures which consists of corner-sharing SiO_4- and AlO_4-tetrahedra that form large cavities and/or channels in the crystals. The channels can be one dimensional (MOR), two dimensional, or three dimensional (FAU). (We refer to dimensions as the number of directions in which molecules can move.) The sizes of the channels and cavities are comparable to those of small molecules/metal clusters.

High resolution electron microscopy (HREM) is a very useful technique to characterize zeolites (*2–4*), even though there is a serious problem with zeolites being very electron beam sensitive materials. The beam stability can be noticably enhanced in two major ways, with a higher Si/Al ratio (or a lower water content) (*5*) and with a higher accelerating voltage of the electrons. It has also been found that a zeolite with confined materials in the channels/cavities tends to have a better beam stability (*2, 6*).

Zeolites are being used as containers for molecular clusters (*6, 7*) and such materials should be characterized before and after incorporation of the clusters. The local information, on an atomic scale, can only be obtained by HREM together with electron diffraction studies. It is possible to get information about the distribution of guest mole-

*To whom correspondence should be addressed.

0022-4596/93 $5.00

cules in the zeolite lattice (*6*) and also to examine if the zeolites are still crystalline after the incorporation.

The type of information that we are interested in is on an atomic scale; i.e., the fine details in the micrographs are essential. Hence, the microscope needs to have a high resolution. The contrast transfer function (CTF), that determines the resolution of the microscope, can be changed in two ways. The zero-cross of the CTF determines the structural resolution limit (r) of the microscope. The resolution depends on the spherical abberation (C_s) of the objective lens and the wavelength (λ) of the electrons (which decreases with an increase of the accelerating voltage) and is given by (*8*)

$$r = 0.66 C_s^{1/4} \lambda^{3/4}.$$

As the stability of the zeolites is enhanced with higher voltage a higher resolution is thus preferably obtained by means of a shorter wavelength.

In this work another problem, that is encountered when zeolites are imaged in certain directions with HREM, is described. Micrographs taken with the large channels aligned parallel to the electron beam are severely disturbed by an artifact. This is seen as a dark spot in the center of the unoccupied channels (*9*).

Earlier works have shown that small metal particles can be imaged with conventional HREM when the zeolite has disintegrated or by using minimum contrast conditions (*10*). Metal particles have also been detected by STEM but also in this case the information from the zeolite lattice is lost due to beam damage (*11*). The aim here is to locate confined material in relation to the zeolite framework structure. It will here be shown that such information can be obtained. With experimental micrographs and image simulations the existence of the artifact spot is pointed out and also how it complicates the interpretation of images. The problem can be avoided by choosing experimental conditions other than the ones ordinarily used for HREM. Two cases are described, MOR which represents the zeolites with one-dimensional channels and FAU which has a three-dimensional channel system.

Experimental and Image Simulations

The microscope used was a JEM-4000EX operated at 400 kV. It has a spherical abberation of 1.0 mm and a structural resolution limit (r) at 1.6 Å. The micrographs were recorded at 150,000–200,000 times magnification on electron microscopy film from Kodak (SO-163). A TV camera with an image intensifier (Gatan, 622) was used to allow focusing at a low electron beam intensity. The electron dose used during focusing was about 10–20 electrons/(sec · Å^{-2}) and a slightly higher dose was needed for film exposure (20–30 electrons/(sec · Å^{-2})). The films were underexposed (4 sec instead of 20 sec) because of the zeolites' limited lifetime in the electron beam. The micrographs were recorded in focus series with steps of 100 or 200 Å.

The zeolite samples were prepared by grinding the powder under methanol or ethanol in an agate mortar and were then collected on a holey carbon grid.

The image simulations were made with the multislice method, using the SHRLI programs (*12*) on a personal computer. The slice thicknesses were put between 1.5 and 2.0 Å. Microscopy parameters corresponding to the microscope were used; accelerating voltage = 400 kV, spherical abberation = 1.0 mm, semiangle of incident beam convergence = 0.3 mrad, and halfwidth of Gaussian spread of defocus = 70 Å. The number of beams used in the multislice calculations were 1427 for MOR and 1139 for FAU. The size of the objective aperture was put to 0.7 Å^{-1}. The experimental images lose some details during irradiation because of some loss in crystallinity and also if there are some mechanical vibration of the microscope. For this reason a vibration parameter was used in the programs. Different values of this parameter were tested (Fig. 1) and

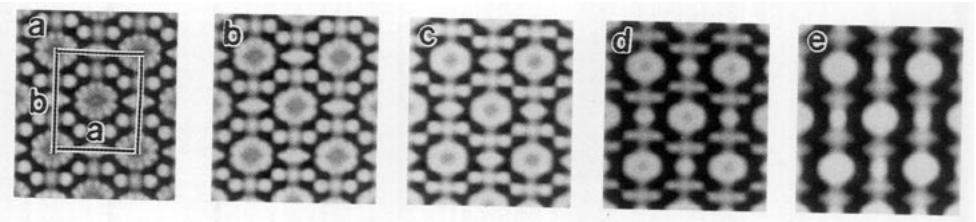

FIG. 1. Simulated images of MOR along [001] with different magnitude of the vibration parameter (VIB) used in the SHRLI programs. The focus is 500 Å and the thickness is 45 Å. (a) VIB = 0 Å, (b) VIB = 0.4 Å, (c) VIB = 0.8 Å, (d) VIB = 1.2 Å, and (e) VIB = 1.6 Å. Images calculated with VIB = 0.8 Å correspond most closely to the experimental micrographs. The unit cell is outlined (a = 18.1 Å and b = 20.5 Å).

the one imposing the best match between the simulated images and the experimental ones was used in the simulations.

In Table I, information about crystal structure and composition of the zeolites is listed (*1*, *13–15*). The channels of FAU are formed by supercages (*16*) linked together. This creates zigzag shaped channels with a center slightly displaced from the center of the supercages. In MOR the channels are straight.

The CTF's were calculated by the EMS programs (*17*). We will refer to the underfocus condition with a positive value.

Results and Discussion

Figure 2 shows the dependence of HREM images of MOR as a function of specimen thickness at Scherzer focus. The thickness dependence is not very drastic in this wide range (15–105 Å) and the experimental images obtained in this work are most likely very thin, at least the outmost edges (within the interval of Fig. 2). The simulated images were therefore calculated for a thickness around 45 Å. Zeolite frameworks are weak electron scatterers, as they contain only light elements (Si, Al and O) with small atomic scattering factors. A discussion based on a weak-phase object approximation (thin crystal and weak scatterer) may thus be informative. By considering the CTF we can then say to what extent each Bragg reflection has been transferred to the image formation. The appearance of the CTF changes with defocus, and consequently the contribution to the image formation from each Bragg reflection will be altered in magnitude and in some cases in phase.

Zeolites have large unit-cell dimensions (10–20 Å); reflections with small scattering vectors will thus have large structure factors and be important for creating an image with a close correspondence to the projected potential. Many of these reflections are essen-

TABLE I

STRUCTURE INFORMATION AND ELECTRON BEAM INCIDENCE FOR MOR AND FAU

Zeolite	Space group	Cell parameters	Si/Al ratio	Incidence direction
Mordenite (MOR)	*Cmcm* Orthorhombic	a = 18.1 Å b = 20.5 Å c = 7.5 Å	≈12	[001]
Faujasite (FAU)	*Fd3m* Cubic	a = 24.3 Å (*15*)	≈∞	[110]

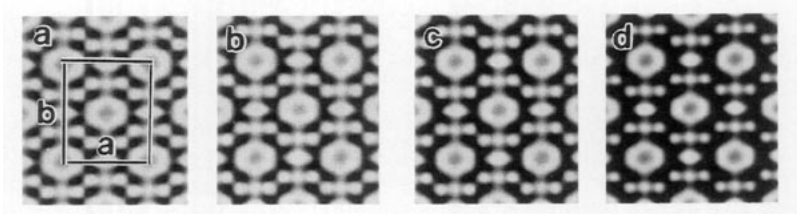

FIG. 2. Simulated images of MOR along [001] at a defocus of 500 Å for different thicknesses. (a) 15, (b) 45, (c) 75, and (d) 105 Å. The images do not change significantly in this rather large thickness interval. Further simulations were made for both zeolites at a thickness of about 45 Å. The unit cell is outlined (a = 18.1 Å and b = 20.5 Å).

tial for generating the contrast in the zeolite channels, because the channels are regularly arranged with a period comparable to the cell parameters. Considering the CTF (Fig. 5) at approximately Scherzer focus condition (500 Å), it is evident that reflections at small reciprocal distances are very poorly transferred by the objective lens.

The Bragg reflections are, for simplicity, divided in two subgroups depending on their phases. Reflections which contribute to light contrast in the center of the channels are called L-reflections and those with a phase difference of π compared to the L-reflections and which thus create a dark contrast are called D-reflections. An image with the closest correspondence to the projected potential would be an image in which information of the reflections was transferred without changing their relative magnitudes. Such a situation is not possible to achieve in an electron microscope but can be obtained by image processing of observed electron micrographs (*18*). Nevertheless, the amount of transfer for the reflections in the microscope can be modified by changing the defocus and a contrast corresponding more closely to the projected potential in the center of the channels can be produced.

Untreated Zeolites

In Tables II and III the Bragg reflections, which are most important for creating the image contrast of the channels, are listed. The tables also show whether the reflections are L- or D-reflections and the number of equivalent reflections lying on the reciprocal

TABLE II

THE MOST IMPORTANT BRAGG REFLECTIONS FOR IMAGING MOR

	Bragg reflection	Amplitude	Type L/D	d^* Å^{-1}	Number of reflections
a	(1, 1, 0)	1.0734	L	0.073	4
b	(0, 2, 0)	1.1798	L	0.098	2
c	(2, 0, 0)	2.4892	L	0.110	2
d	(1, 3, 0)	0.7302	L	0.156	4
e	(3, 1, 0)	0.8726	D	0.173	4
f	(3, 3, 0)	1.6822	D	0.221	4

Note. The amplitude, type (if they are light- or dark-forming), and the length of the scattering vectors (d^*) are also shown. The last column mentions how many structurally related reflections contribute to image formation in the [001] direction.

TABLE III

THE MOST IMPORTANT BRAGG REFLECTIONS FOR IMAGING FAU

	Bragg reflection	Amplitude	Type L/D	d^* Å^{-1}	Number of reflections
a	(−1, 1, 1)	1.4436	L	0.070	4
b	(−1, 1, 3)	0.5529	L	0.134	4
c	(−3, 3, 1)	0.8201	D	0.176	4
d	(−1, 1, 5)	0.5028	D	0.210	4
e	(−3, 3, 5)	0.7975	D	0.265	4

Note. The amplitude, type (if they are light- or dark-forming), and the length of the scattering vectors (d^*) are also shown. The last column mentions how many structurally related reflections contribute to image formation in the [110] direction.

plane that contribute to image formation in the electron beam directions considered.

Mordenite (*MOR*). Figure 3 shows a through focus series (steps 200 Å) of micrographs of MOR taken with [001] incidence. The crystal thickness increases so rapidly that only the outmost edge can be considered. The image in Fig. 3a is recorded at conditions very close to Scherzer focus as can be judged by the good fit with the simulated image calculated for the focus of 500 Å. The spots in the channels are very strong, but they get weaker as the focus is lowered, as can be seen in Fig. 3b (approximately 700 Å), and will finally almost disappear at 900 Å (Fig. 3c).

Two sets of reflections, *e* and *f* (Table II), are the most important for creating the dark contrast in the channel because of their high transfer at 500 Å (Fig. 5). The four L-

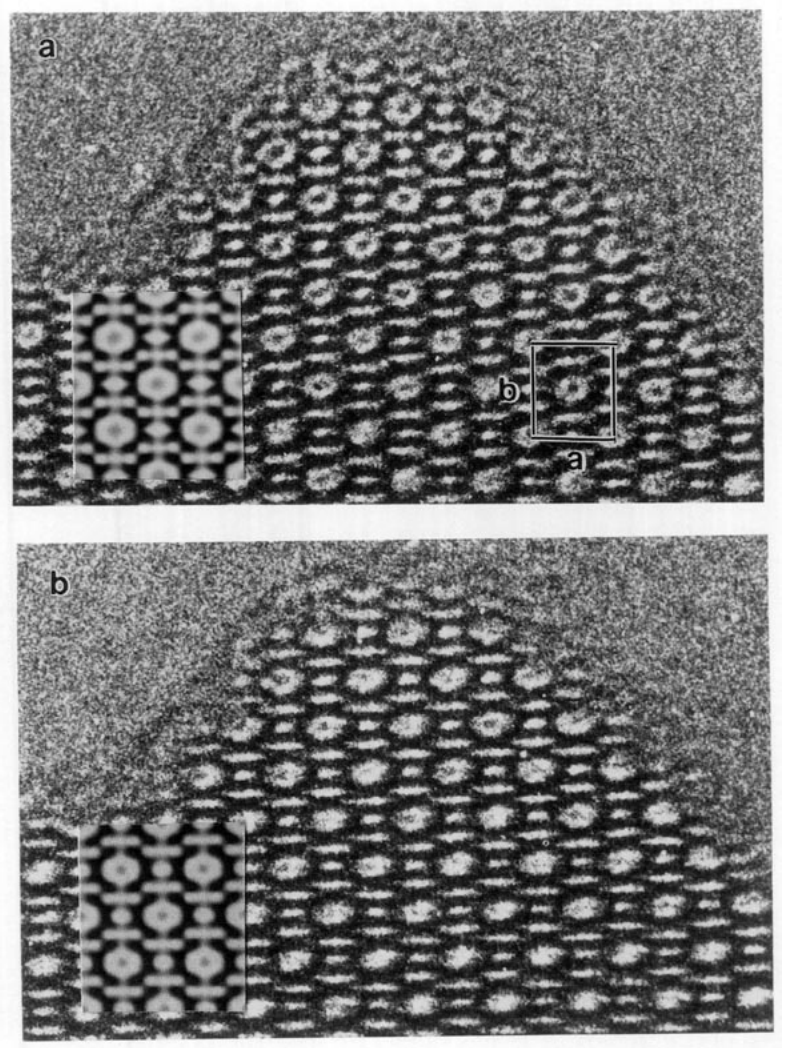

FIG. 3. Micrographs of a crystal of MOR recorded with the electron beam parallel to [001]. The focus values are approximately 500 (a), 700 (b), and 900 Å (c). Inserted are the simulated images at these focuses calculated for a thickness of 45 Å. The crystal gets thicker very quickly so only the edge is interpretable. The spot contrast weakens when the focus is lowered. The unit cell is outlined (a = 18.1 Å and b = 20.5 Å).

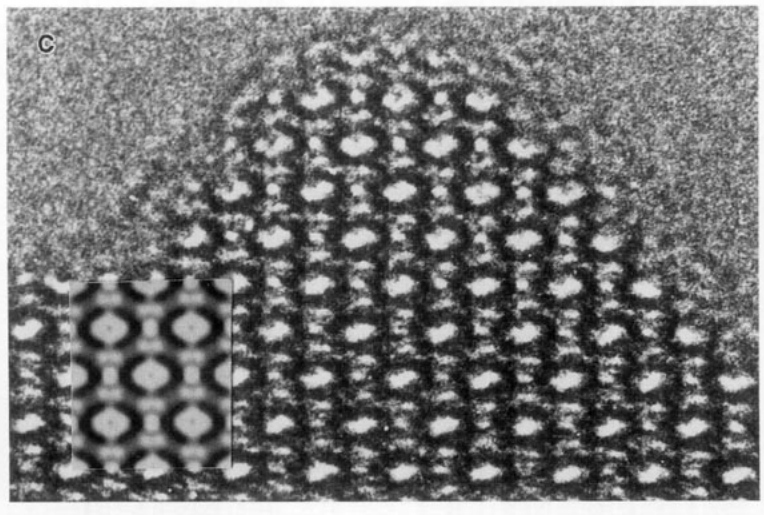

FIG. 3—*Continued*

reflections mentioned have low transfer at this focus. This makes the dark contrast outweigh the light one resulting in the apparition of the spots. The spots disappear quite quickly when going to a lower underfocus (Fig. 4). At 900 Å the spots are very weak and at 1000 Å they have vanished completely. The *f*-reflections, which are the strongest D-reflection, have lost some transfer at 1000 Å at the same time as the L-reflections all have enhanced their transfer. This is enough, as can be seen in Fig. 4k,

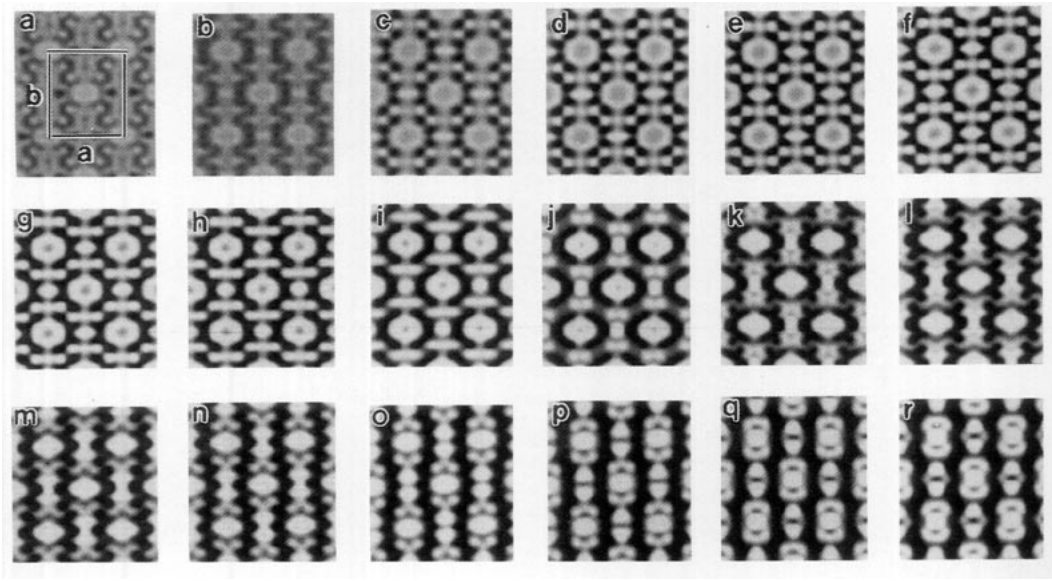

FIG. 4. Simulated images of MOR along [001] at a crystal thickness of 45 Å and the following focuses (a) 0, (b) 100, (c) 200, (d) 300, (e) 400, (f) 500, (g) 600, (h) 700, (i) 800, (j) 900, (k) 1000, (l) 1100 (m) 1200, (n) 1300, (o) 1400, (p) 1500, (q) 1600, and (r) 1700 Å. The dark spots which are obvious at focuses close to 500 Å are gone at 1000 Å. Still lower focuses give images where the channels are easily discerned. The unit cell is outlined (a = 18.1 Å and b = 20.5 Å).

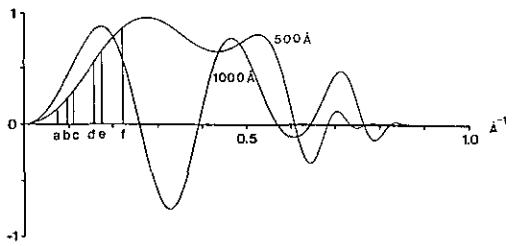

FIG. 5. The CTF calculated for 500 and 1000 Å. The location of the Bragg reflections for MOR listed in Table II (*a*, *b*, *c*, *d*, *e*, and *f*) are marked. All reflections except *f* are more strongly transferred at 1000 than at 500 Å. The *f*-reflection, which is the most important D-reflection, is, however, weaker. This results in the fact that the dark spot is absent at this focus.

to remove the spots. At still lower focuses the position of the channels can easily be found without artifact spots.

Zeolite Y (FAU). The center of the channels does not coincide in projection with the center of the supercages. The spots are located in the center of the channels as can be seen in Fig. 6a. The micrograph shows a crystal of FAU with the simulated image at 500 Å inserted in the lower right corner. In Fig. 6b, recorded after Fig. 6a, the crystal is damaged by the electrons and the image has lost some details. The simulated image at 1000 Å, which corresponds most closely to the micrograph, is inserted.

A series of simulated images for FAU are shown in Fig. 7. The spots in the channels, which are very strong in the images close to Scherzer focus, become weaker when the focus is lowered. Three sets of reflections, *c*, *d*, and *e* (Table III), contribute mainly in producing the dark contrast. Reflections *a* and *b* are L-reflections. When lowering the focus from Scherzer focus the first four sets of reflections will obtain a better transfer while the *e*-reflection will start to lose transfer (Fig. 8). A poorer transfer will also be the result for the *d*-reflections, which at 900 Å, will have the same transfer as at Scherzer. Further lowering of the focus will diminish the *d*-reflections even more and the spots will accordingly get weaker and disappear completely at 1100 Å. The shape of the channels is altered at around 1000 Å, from being round or elliptical; they now start to get a kind of waist. This gets even more pronounced at still lower focuses.

Zeolites with Iron Cluster

Computer image simulations were also made with small (six atoms) iron clusters in the zeolite channels. The iron serve as a model for the possibility of detecting confined materials. For MOR the clusters were placed in the center of the channels and for FAU they were placed in the center of the supercages. As pointed out earlier this position in projection is not the same as the position of the spots and the clusters are not expected to be obscured in the same way as in MOR. The iron constitute approximately 15 (MOR) and 20 wt% (FAU) of the total weight of the zeolite with iron cluster.

Mordenite (MOR). The iron atoms were placed in an octahedron in the channel (in special positions (0.0, 0.0, 0.237), (0.098, 0.0, 0.0), and (0.0, 0.87, 0.0) with half occupancy). There are 12 Fe atoms in each unit cell and 48 Si. The contrast caused by the iron cluster is more distinct than the spots in the empty MOR. The images for MOR with Fe change quite drastically at about 900 Å (Fig. 9). It is no longer clear where the channels are situated. There is a pronounced difference at 900 Å between the unoccupied (Fig. 4j) and the iron MOR (Fig. 9j). To determine whether or not the crystal contains confined material it is necessary to image it at a focus condition between 600 and 900 Å. A focus series would be more instructive as the size of the spot does not change when it is caused by confined material as it does when it is an artifact.

Zeolite Y (FAU). The problem of locating materials in FAU has been discussed in some earlier works. Chan *et al.* (*19*) have from studies of simulated images reported that small Pt-clusters in FAU cannot be detected simulated-image studies at least not in a 200 kV microscope. In that case the cluster was placed in the center of the channels. It has been found possible to detect

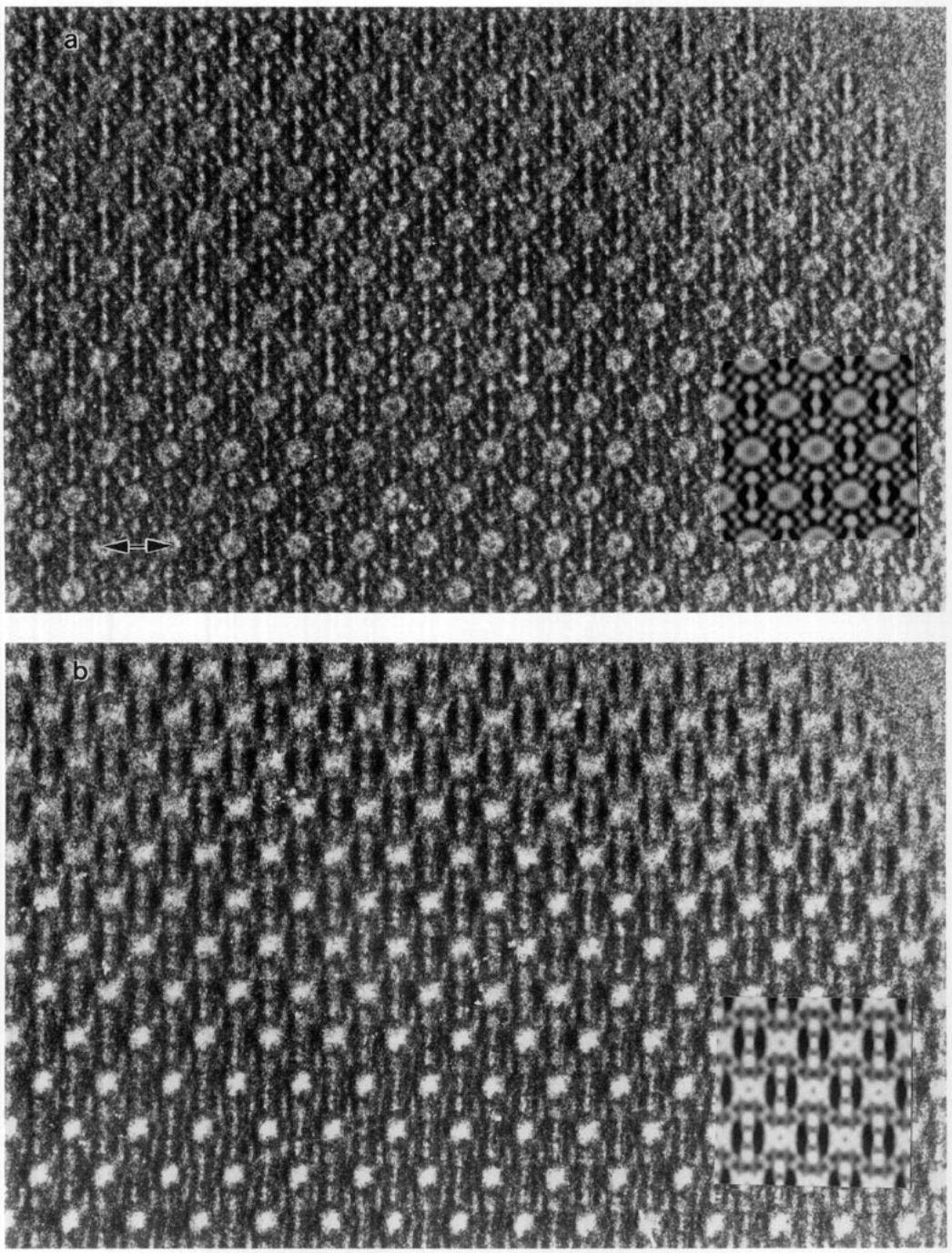

FIG. 6. Micrographs of a FAU crystal recorded at two focus values, approximately 500 (a) and 1000 Å. (b). Inserted are the simulated images at these focuses calculated for a thickness of 44 Å. The micrograph at 1000 Å, taken after the one at 500 Å, is damaged by the electron beam. The beam incidence is [110]. Scale bar = 15.2 Å.

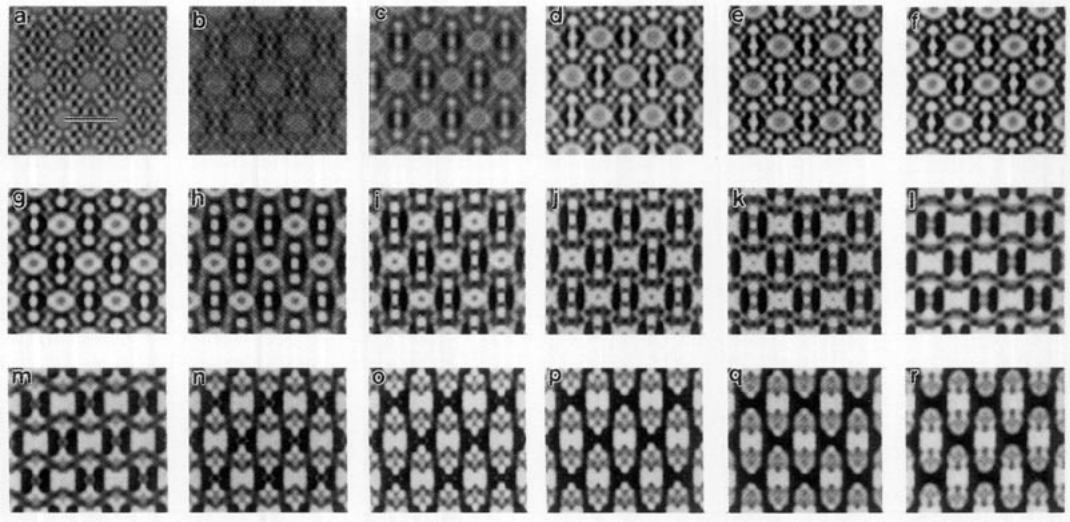

FIG. 7. Simulated images of FAU along [110] calculated for a crystal thickness of 44 Å and the focuses (a) 0, (b) 100, (c) 200, (d) 300, (e) 400, (f) 500, (g) 600, (h) 700, (i) 800, (j) 900, (k) 1000, (l) 1100, (m) 1200, (n) 1300, (o) 1400, (p) 1500, (q) 1600, (r) 1700 Å. The spots in the channels remain visible down to a focus of 1000 Å after which the appearance of the images changes drastically. Scale bar = 15.2 Å.

confined selenium in FAU by observing the crystals in the [211] direction (*20*). We will here concentrate on the possibility of detecting materials confined in the center of the supercages of FAU by observation along the [110] direction.

48 iron atoms were placed in the unit cell (in positions 48*f* (0.553, $\frac{1}{8}$, $\frac{1}{8}$) based on the space group $Fd\bar{3}m$) which contains 192 atoms of Si. They constitute an octahedra in the center of the supercages. The simulated images change appearance drastically when the iron is implanted. By comparing the simulated images with (Fig. 10), and without Fe (Fig. 7), it is clear that confined materials in the centers of the supercages noticably change the images, except at 1100 Å.

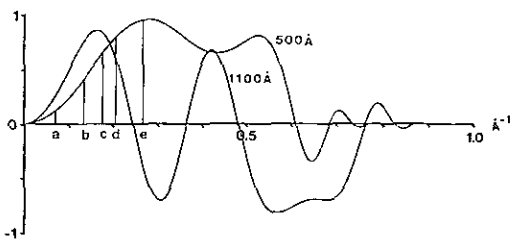

FIG. 8. The CTF for 500 and 1100 Å. The location of the Bragg reflections for FAU listed in Table III (*a*, *b*, *c*, *d* and *e*) are marked. At 1100 Å the *c*- and *d*-reflections (*D*) have a poorer transfer than at 500 Å while the others are more strongly transferred.

Conclusion

In an earlier work (*21*) we discussed the artifact spot problem for the zeolite silicalite I (MFI). It was solved by using a low underfocus (800 Å) and by cutting off higher order reflections with a suitable objective aperture. We have now found that higher order reflections tend to cancel out each other so it is not necessary to use the smaller objective aperture, just lowering the focus seems to be sufficient. This seems to be valid for MOR which have straight channels and maintain a quite interpretable image of the structure when the focus is lowered. For FAU, which have zigzag shaped channels, the situation is slightly different. This can be seen in the simulated images, Fig. 7, which change appearance considerably with focus change.

We have shown that materials confined in the zeolite spaces of MOR and FAU can

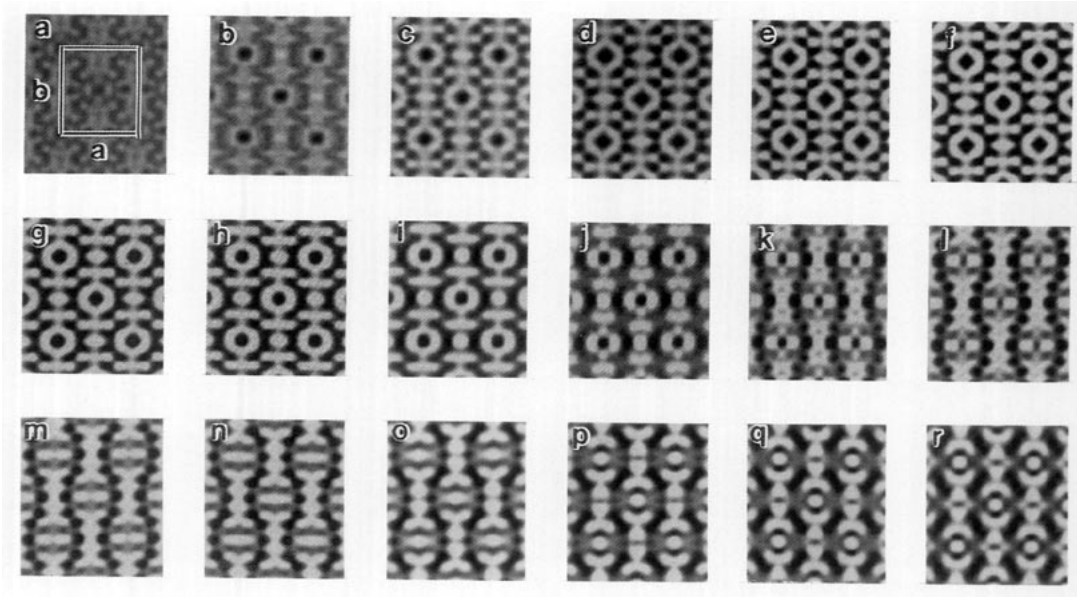

FIG. 9. Simulated images of MOR, with iron clusters in the channels, along [001], calculated for a thickness of 45 Å. The following focuses were calculated (a) 0, (b) 100, (c) 200, (d) 300, (e) 400, (f) 500, (g) 600, (h) 700, (i) 800, (j) 900, (k) 1000, (l) 1100, (m) 1200, (n) 1300, (o) 1400, (p) 1500, (q) 1600, and (r) 1700 Å. The images correspond approximately to the projected potential down to a focus of 800 Å. Then the images are very difficult to interpret. The unit cell is outlined (a = 18.1 Å and b = 20.5 Å).

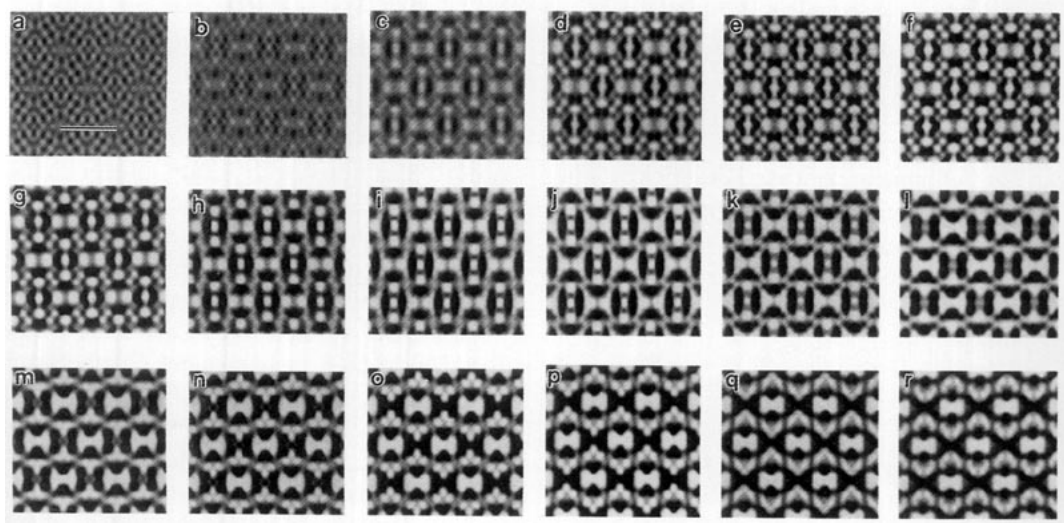

FIG. 10. Simulated images of FAU, with iron clusters in the center of the supercage, along [110], calculated for a thickness of 44 Å. The following focuses are calculated (a) 0, (b) 100, (c) 200, (d) 300, (e) 400, (f) 500, (g) 600, (h) 700, (i) 800, (j) 900, (k) 1000, (l) 1100, (m) 1200, (n) 1300, (o) 1400, (p) 1500, (q) 1600, and (r) 1700 Å. The images are very different from the ones without iron clusters (Fig. 7), except at focuses close to 1100 Å. Scale bar = 15.2 Å.

be detected with HREM and similar results were obtained for MFI and zeolite Linde L (LTL). For these four types of zeolites there are in all cases quite distinctive differences between the empty zeolites and the zeolites with iron clusters confined in their cavities/channels. The contrast problem with the artifact spots which we described in the first part of this work can be avoided by working at other microscopic parameters than are normally used. This simple argument is valid for MOR (and LTL and MFI) with straight channels parallel to the incident electron beam. For FAU the position of the confined material does not necessarily coincide with the position of the spots and this will make the problem different from those of the other zeolites.

In our calculations we used iron as a model for the confined material. This is a rather heavy scatterer compared to the constituents of the zeolite framework but a moderate scatterer compared to many other elements used for catalysts like Pt or Rh. We can therefore expect a lesser amount of material to be detectable provided it consists of heavy scattering atoms.

Acknowledgments

Professor Sten Andersson is acknowledged for encouragement and discussion. This work was supported with grants from the Swedish Natural Science Research Council and the Swedish National Energy Administration.

References

1. W. M. Meier and D. H. Olson, "Atlas of Zeolite Structure Types," 2nd revised ed., Structure Commission of the International Zeolite Association, Butterworths, London (1987).
2. O. Terasaki, *Acta Chem. Scand.* **45,** 785 (1991).
3. O. Terasaki, J. M. Thomas, G. R. Millward, and D. Watanabe, *Chem. Mater.* **1** (1), 158 (1989).
4. J. M. Newsam, M. M. J. Treacy, W. T. Koetsier, and C. B. de Gruyter. *Proc. R. Soc. London A* **420,** 375 (1988).
5. L. A. Bursill, J. M. Thomas, and K. J. Rao. *Nature* **289,** 157 (1981).
6. O. Terasaki, K. Yamazaki, J. M. Thomas, T. Ohsuna, D. Watanabe, J. V. Sanders, and J. C. Barry, *J. Solid State Chem.* **77,** 72 (1988).
7. V. N. Bogomolov. *Sov. Phys. Usp.* **21,** 77 (1978).
8. O. Scherzer. *J. Appl. Phys.* **20,** 20 (1949).
9. M. A. O'Keefe and J. V. Sanders. *Optik* **46,** 421 (1976).
10. M. Pan, J. M. Cowley, and I. Y. Chan. *Catal. Lett.* **5,** 1 (1990).
11. S. B. Rice, J. Y. Koo, M. M. Disko, and M. M. J. Treacy. *Ultramicroscopy* **34,** 108 (1990).
12. M. A. O'Keefe and P. Buseck. *Trans. Am. Crystallogr. Assoc.* **15,** 27 (1979).
13. W. M. Meier, Z. *Kristallogr.* **115,** 439 (1961).
14. Structure reports, Vol. pp. 29, 404–405, A. Oosthoek's Uitgeversmaatschappij N. V. Utrecht (1964).
15. D. Klint, private communication.
16. D. W. Breck, "Zeolite Molecular Sieves," Wiley, New York (1974).
17. P. A. Stadelmann, *Ultramicroscopy* **21,** 131 (1978).
18. V. Alfredsson, O. Terasaki, and D. Shindo, "Electron Microscopy" (A. Lopez-Galindo and M. I. Rodriguez-Garcia, Eds.), EUREM 92, Vol. 2, Univ. of Granada, Granada, Spain (1992).
19. I. Y. Chan, R. Csencsits, M. A. O'Keefe, and R. Gronsky. *J. Catal.* **103,** 466 (1987).
20. O. Terasaki, K. Yamazaki, J. M. Thomas, and D. Watanabe. *Inst. Phys. Conf. Ser.* **93,** 297 (1988).
21. V. Alfredsson, O. Terasaki, and J.-O. Bovin. *J. Solid State Chem.* **84,** 171 (1990).